



Significant enhancement of the visible photocatalytic degradation performances of γ -Bi₂MoO₆ nanoplate by graphene hybridization

Feng Zhou^{a,b,*}, Rui Shi^a, Yongfa Zhu^a

^a Department of Chemistry, Tsinghua University, Beijing 100084, PR China

^b Department of Materials Science and Engineering, Dalian Maritime University, Dalian 116026, PR China

ARTICLE INFO

Article history:

Received 7 January 2011

Received in revised form 11 March 2011

Accepted 16 March 2011

Available online 31 March 2011

Keywords:

Graphene

γ -Bi₂MoO₆

Hybridize

Photocatalyst

Visible light irradiation

ABSTRACT

After hybridized with graphene, the photocatalytic performances of γ -Bi₂MoO₆ were increased about 2–4 times. The photocatalytic activity enhancements were dependent on the amount of graphene and it was found that the optimal hybridized amount of graphene was about 1.0 wt%, which was close to the monolayer disperse of graphene on γ -Bi₂MoO₆ surface. The mechanism on the enhancement of photocatalytic activity is attributed to the higher separation efficiency of photo-induced electrons and holes, which come from the electronic interaction between γ -Bi₂MoO₆ and graphene. The electronic interaction was verified by the photoelectrochemical measurements.

© 2011 Elsevier B.V. All rights reserved.

1. Introduction

Photocatalysis has attracted worldwide attention because of its potential applications in water splitting and the degradation of organic compounds [1,2]. Since visible-light takes up ca. 43% of the solar energy while UV light only ca. 4%, developing visible-light responsive photocatalysts is becoming a promising and challenging research area at the present time [3]. Due to the potential excellent photocatalytic property under the visible light, the γ -Bi₂MoO₆ (BMO) has attracted extensive attention these days [4–7]. The γ -Bi₂MoO₆ with the Aurivillius structure has been found to possess unique layered structure in which perovskite slabs of corner-sharing, distorted MoO₆ octahedra are sandwiched between (Bi₂O₂)²⁺ layers [8]. A major limitation to achieve higher photocatalytic efficiency is the quick recombination of photo-generated charge carriers. Recombination has faster kinetics than surface redox reactions and greatly reduces the quantum efficiency of photocatalysis. γ -Bi₂MoO₆ nanoplates have been designed for fast separation and transfer of photoexcited electrons and holes. How to design more highly efficient Bi₂MoO₆-based photocatalysts remains a huge challenge.

Many works have been devoted to reduce the recombination of charge carriers by coupling the photocatalysts with conjugative π structure carbon materials [9,10]. The authors together with other researchers have developed the carbon material hybridized semiconductor as efficient photocatalysts, such as C60 [11,12] and graphite-like carbon [13,14]. Graphene is a two dimensional macromolecular sheet of sp²-bonded carbon atoms that are arranged into a honeycomb structure [15]. Apart from its unique electronic properties, the 2D planar structure material has superior electrical conductivity [16], which would make it an excellent electron-transport material in the process of photocatalysis, even more appropriate than C60 and graphite-like carbon. Moreover, the surface properties of graphene could be adjusted via chemical modification, which facilitates its application in composite materials [17,18]. Thus, a combination of γ -Bi₂MoO₆ and graphene is promising to simultaneously possess excellent transparency, conductivity, and controllability, which could facilitate effective photodegradation of pollutants under visible light. To the authors' best knowledge, there are only few reports focused on this topic. Recently, TiO₂ and ZnO nanoparticles have been dispersed on the graphene sheets, and the composites showed enhanced photocatalytic activity [19,20]. However, the mechanism of the electronic interaction between graphene and semiconductor is still unclear and need further studies.

In this work, the authors demonstrated a facile route to obtain an efficient γ -Bi₂MoO₆ photocatalyst by graphene hybridization. The photodegradation results of dyes over graphene hybridized with Bi₂MoO₆ show that the photocatalytic activity can be sig-

* Corresponding author at: Department of Materials Science and Engineering, Dalian Maritime University, Dalian 116026, PR China. Tel.: +86 411 84723586; fax: +86 411 84725960.

E-mail address: zhoufeng99@mails.tsinghua.edu.cn (F. Zhou).

nificantly enhanced under visible-light irradiation. It is postulated that the enhanced photoactivity of graphene-hybridized Bi_2MoO_6 catalyst results from high migration efficiency of photoinduced electron–hole pairs. The structure and interfacial electronic interaction between $\gamma\text{-Bi}_2\text{MoO}_6$ and graphene, as well as its effect on the photocatalytic activity were systematically investigated.

2. Experimental

2.1. Materials preparation

$\gamma\text{-Bi}_2\text{MoO}_6$ was synthesized by the hydrothermal method. In a typical procedure, 2.5 mmol of $\text{Na}_2\text{MoO}_4 \cdot 2\text{H}_2\text{O}$ and 5 mmol of $\text{Bi}(\text{NO}_3)_3 \cdot 5\text{H}_2\text{O}$ were respectively dissolved in 35 mL of distilled water, and then transferred into a 50 mL Teflon-lined stainless steel autoclave. The autoclave was sealed and maintained at 180°C for 24 h, then cooled to room temperature naturally. Graphene oxide (GO) was prepared from nature graphite by the reported method [21]. All chemicals used were reagent grade without further purification. Preparation of graphene hybridized Bi_2MoO_6 was realized in two steps. Firstly, appropriate as-prepared graphite oxide was dispersed in water to achieve 0.05 wt% dispersion. Exfoliation of graphite oxide to GO was obtained by ultrasonication of the dispersion for 30 min and 1 g Bi_2MoO_6 was added into the GO dispersion. Then Bi_2MoO_6 and GO mixture was dispersed by ultrasonication for 30 min and stirred for 24 h. The suspension was filtrated and the precipitate was washed with deionized water three times, and then transferred to an oven to dry at 80°C for 24 h; herein, a series of GO- Bi_2MoO_6 powders from 0.5 to 4.0 wt% were synthesized. The second step was the reduction of GO to graphene which was performed according to the literature [22,23]. Appropriate GO- Bi_2MoO_6 powder was dispersed in water and ultrasonicated for 30 min. In a typical procedure, appropriate amount of ammonia solution (28 wt% in water) and hydrazine solution (35 wt% in water) were added to the above dispersion. The weight ratio of hydrazine to GO was about 7:10. After being stirred for a few minutes, the dispersion was put in a water bath (95°C) for 1 h. Finally, the resulting composite was recovered by filtration, rinsed by deionized water several times, and evaporated at 80°C for 10 h.

2.2. Characterization

Diffusion reflection spectra (DRS) measurements were carried out on a Hitachi U-3010 instrument with BaSO_4 as the reference sample. High resolution transmission electron microscopy (HRTEM) images were obtained by JEM 2010F field emission transmission electron microscope with an accelerating voltage of 200 kV. Raman spectra were recorded on a microscopic confocal Raman spectrometer (Renishaw 1000 NR) with an excitation of 514.5 nm laser light. Photoelectrochemical properties were measured on an electrochemical system (CHI-660B, China).

2.3. Photocatalytic experiments

The photocatalytic activity was evaluated by the degradation of methylene blue (MB) under visible light irradiation ($\lambda > 420\text{ nm}$). The visible light was obtained by a 500 W xenon lamp (Institute of Electric Light Source, Beijing) with a 420 nm cutoff filter to ensure that the desired irradiation light was obtained. The average light intensity was 31.2 mW cm^{-2} measured by a power meter from the Institute of Electric Light Source, Beijing. 50 mg of graphene-hybridized Bi_2MoO_6 photocatalysts were dispersed in a 100 mL MB suspension ($1 \times 10^{-5}\text{ M}$). The suspensions were magnetically stirred in the dark for 30 min to reach the absorption–desorption equilibrium before the irradiation. At certain time intervals, 2 mL aliquots were sampled and centrifuged to remove the particles. The

filtrates were analyzed by recording variations in the absorption band (664 nm) in the UV–vis spectra of MB using a Hitachi U-3010 UV-Vis spectrophotometer. The active oxidants generated in the photocatalytic process could be measured through trapping by disodium ethylenediamine tetraacetate (EDTA-2Na) and tert-butyl alcohol (t-BuOH). Here 1 mM t-BuOH was introduced to scavenge the hydroxyl radicals and investigated the role of free radicals during the photodegradation process in the present of graphene-hybridized BMO samples. On the other hand, the trapper of the photogenerated holes (1 mM EDTA-2Na) was added into the suspensions to study whether the holes were the main active oxidative species. The suspensions were stirred in the dark for 30 min before the irradiation, and the photocatalytic activities of the samples were tested by the degradation of MB.

2.4. Photoelectrochemical measurements

Photoelectrochemical tests were carried out in a conventional three-electrode, single-compartment quartz cell, filled with 0.1 M Na_2SO_4 electrolyte, using a potentiostat. The ITO/ Bi_2MoO_6 or ITO/graphene- Bi_2MoO_6 electrodes served as the working electrode. The counter and the reference electrodes were platinum gauze and saturated calomel electrode (SCE), respectively. A 500 W xenon lamp with a 420 nm cutoff filter (the average light intensity was 31.2 mW cm^{-2}) was used as the source of visible light irradiation.

3. Results and discussion

3.1. Enhancement of photocatalytic activity

The photocatalytic activities of Graphene- Bi_2MoO_6 (G-BMO) photocatalysts were measured by the photodegradation of methylene blue (MB) as model reaction under visible light ($\lambda > 420\text{ nm}$), and the results were shown in Fig. 1A. It can be seen that the visible light activity has been enhanced for all Graphene- Bi_2MoO_6 samples, compared to the reference photocatalyst. In this system, the photodegradation process followed pseudo-first-order kinetics procedure, and it can be explained in a Langmuir–Hinshelwood model. When solution was diluted, the reaction rate could be expressed by $r = kKC$, where K referred to adsorption equilibrium constant, k was reaction constant, and C was the concentration of the reactant. The influence of the amounts of graphene hybridized upon the photodegradation rate of MB was shown in the inset of Fig. 1. Pure Bi_2MoO_6 presents an apparent reaction rate constant k of 0.0037 min^{-1} , while the sample of Bi_2MoO_6 hybridized with 0.5 wt% of graphene showed an apparent reaction rate constant of 0.0091 min^{-1} , which was more than twice faster than Bi_2MoO_6 alone. The sample with 1.0 wt% of graphene showed the highest activity ($k = 0.0136\text{ min}^{-1}$), the activity of MB degradation was increased by almost 4 times after 1.0 wt% of graphene loaded. The inset of Fig. 1A also showed that with the graphene content increasing, the photocatalytic performance of Graphene- Bi_2MoO_6 did not improve monotonously. When the graphene content was relatively low ($< 1.0\text{ wt}\%$), the photocatalytic activity increased continuously. However, when the graphene content was relatively high ($> 1.0\text{ wt}\%$), the photocatalytic activity decreased with increasing graphene content. The optimal loading amount of graphene on the surface of BMO was approximately 1.0 wt%. The decreased activity at higher graphene loading was attributed to the increased absorbance and scattering of photons through excess graphene in the photosystem. Fig. 1B showed the photodegradation rates of MB on graphene, Bi_2MoO_6 , Graphene-BMO composite and mechanical mixture of Bi_2MoO_6 and graphene. Graphene showed negligible photodegradation of MB. The mechanical mixture of

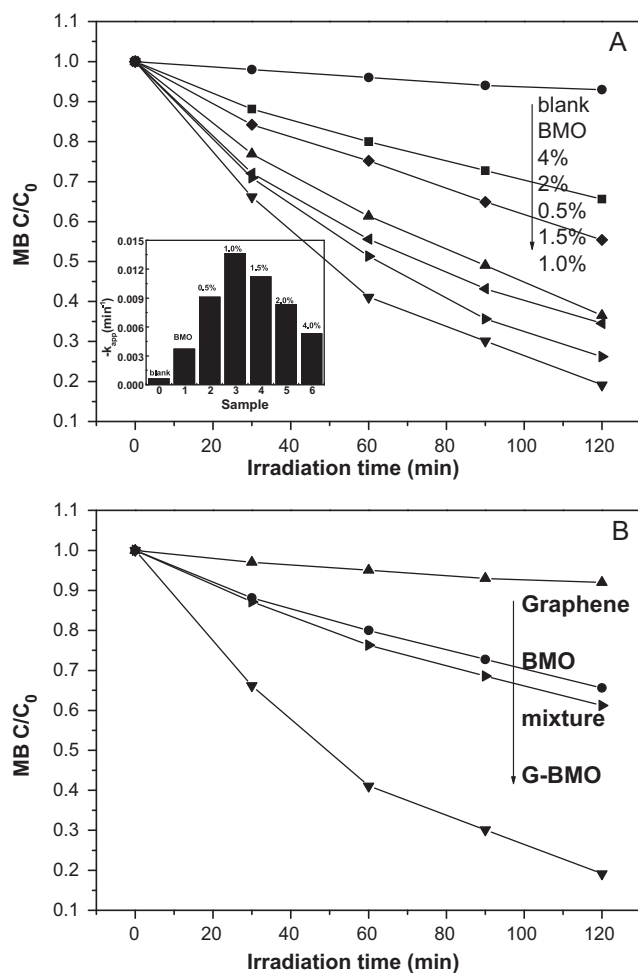


Fig. 1. Photocatalytic degradation of MB over the as-prepared samples under visible light irradiation ($\lambda > 420$ nm): (A) the photodegradation plots and rate constant k as a function of graphene content, (B) photocatalytic degradation of MB over graphene, BMO, mechanical mixture of BMO and graphene (1.0 wt%), and the Graphene–BMO (graphene 1.0 wt%) composite, catalyst loading, 0.5 g L^{-1} ; MB, $1 \times 10^{-5} \text{ M}$.

Bi_2MoO_6 and graphene (1 wt%) showed slightly higher photocatalytic activity than that of pure Bi_2MoO_6 , while the Graphene–BMO composite with the same amount of graphene loading possessed a much higher activity. The 4 times higher activity of Graphene–BMO composite compared with mechanical mixture of Bi_2MoO_6 and graphene was attributed to the intimate contact between Bi_2MoO_6 and graphene, which was crucial for the for-

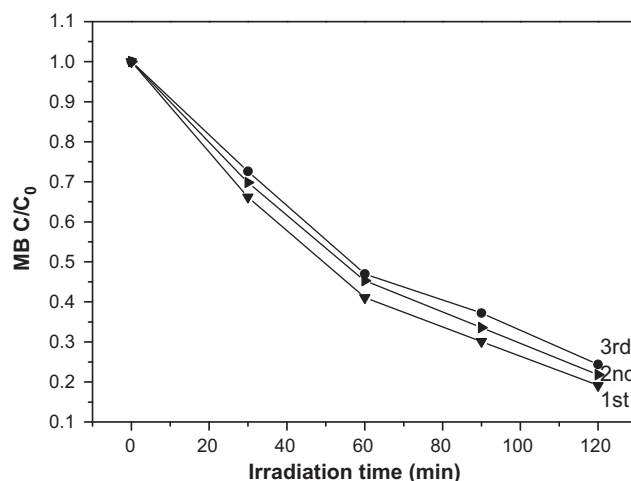


Fig. 2. Removal efficiency of MB with experimental times in the presence of Graphene–BMO photocatalyst under visible light irradiation ($\lambda > 420$ nm).

mation of electronic interaction and interelectron transfer at the interface.

An attractive feature of the photocatalyst materials was that the photocatalytic activity of the photocatalyst was stable. The stability of the photocatalyst was attributed to the chemical interaction between Bi_2MoO_6 and graphene, which enable the graphene stable to the photocatalyst, and the graphene could not be degraded during the photodegradation of methylene blue. Under visible light irradiation, 80% of MB could be degraded over Graphene– Bi_2MoO_6 (1.0 wt%) within 2 h for the first irradiation, and the samples presented stable visible light photocatalytic activity in recycled reaction (Fig. 2). And the Graphene– Bi_2MoO_6 photocatalysts could be easily separated from the MB suspension by simple centrifugation after reaction, which facilitated the reuse of the catalyst.

3.2. Hybrid structures

The hybridization structure of Bi_2MoO_6 and graphene was investigated by HRTEM. The graphene nanosheets and $\gamma\text{-Bi}_2\text{MoO}_6$ nanoplates were clearly observed from Fig. 3A. The image in Fig. 3B showed the intimate contact between Bi_2MoO_6 and graphene. This intimate contact made the electronic interaction between Bi_2MoO_6 and graphene possible, and improved the charge separation and the photocatalytic activity.

DRS patterns of Graphene– Bi_2MoO_6 photocatalysts were shown in Fig. 4. The patterns revealed that compared with the pure Bi_2MoO_6 , graphene-hybridized Bi_2MoO_6 showed almost the same

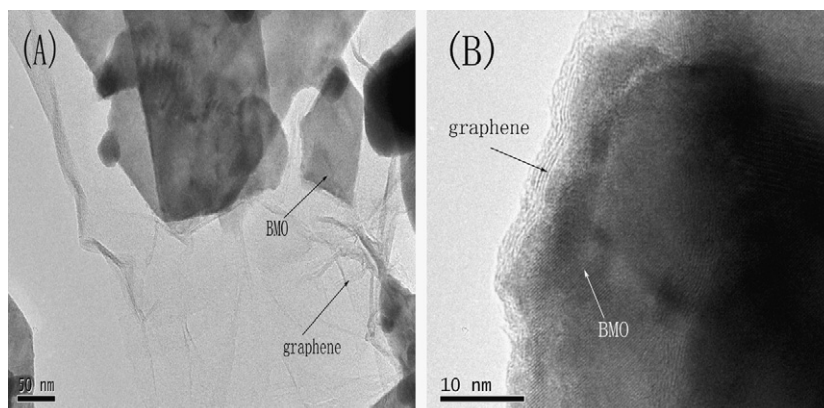


Fig. 3. HRTEM images of G–BMO composite (1.0 wt%).

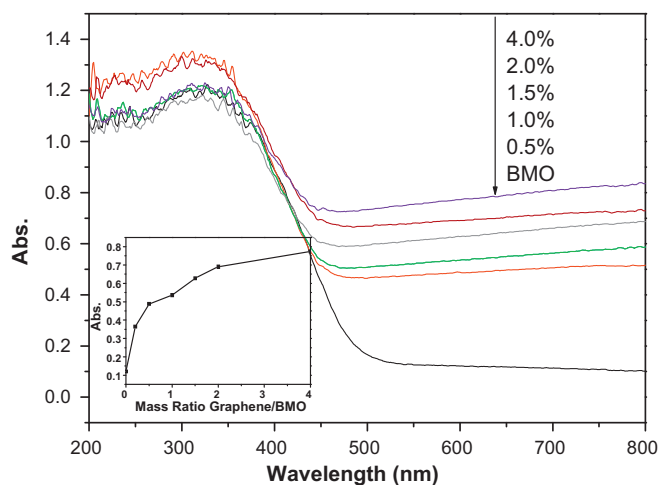


Fig. 4. UV-vis diffuse reflection spectra of BMO and G-BMO samples.

absorbance edge, but extended the absorbance to the whole visible region due to the presence of graphene on Bi_2MoO_6 . The absorption intensity of the prepared samples varied with the increase of the graphene amount. Furthermore, the absorbance of samples at the wavelength of 600 nm changed with a function of mass ratio of graphene/BMO (the inset of Fig. 4). The absorption intensity increased rapidly with the ratio of graphene/ Bi_2MoO_6 from 0.5 to 1.0 wt%, but the increment was insignificant from 1.5 to 4 wt%. Based on the DRS observation and results of photocatalytic activities, it was speculated that the weight ratio at which nearly compact graphene monolayer coverage was formed on the surface of Bi_2MoO_6 was about 1.0 wt%. Graphene may aggregate to form cluster on the surface of Bi_2MoO_6 nanoplates when the weight ratio of graphene/ Bi_2MoO_6 was above 1.0%.

XRD patterns were used to estimate the phase of the samples with different mass ratios of graphene and Bi_2MoO_6 . The patterns of Graphene- Bi_2MoO_6 photocatalysts exhibited similar diffraction peaks as those for $\gamma\text{-Bi}_2\text{MoO}_6$ (See the Supporting Information, Fig. S1).

3.3. Hybridized action between graphene and Bi_2MoO_6

Raman spectra were studied to obtain the information on the interface interaction of Bi_2MoO_6 and graphene. The Raman spectra of Graphene- Bi_2MoO_6 photocatalysts at room temperature and ambient pressure are shown in Fig. 5. The Raman spectrum of Bi_2MoO_6 phase showed a very strong band at 795 cm^{-1} , which was presumably A_{1g} mode, and represented the symmetric stretch of the MoO_6 octahedron [24,25]. All the Graphene- Bi_2MoO_6 samples exhibit the peak around 795 cm^{-1} . It was notable that the Raman peak of the Mo-O stretching bands shifted gradually as the mass ratio of graphene and Bi_2MoO_6 varies. Compared with pure Bi_2MoO_6 , the peak of the Mo-O stretching bands at 795 cm^{-1} was slightly red-shifted by 5 cm^{-1} in the Graphene- Bi_2MoO_6 composites. The relationship between Raman stretching frequency and bond length was found to follow a simple exponential form:

$$R_{\text{Mo-O}} = 0.48239 \ln \left(\frac{32895}{\nu} \right) \quad (1)$$

where ν is the Raman stretching frequency in wavenumbers and R is the metal-oxygen bond length in angstroms [26]. It could be concluded that the lower frequencies of the Raman stretching band correspond to the longer bond lengths. A calculation of the Mo-O bond length for Bi_2MoO_6 based on the expression suggests that one of the Mo-O (apical) bond length (795 cm^{-1}) decreased from 1.796 \AA in Bi_2MoO_6 to 1.793 \AA in the Graphene- Bi_2MoO_6 compos-

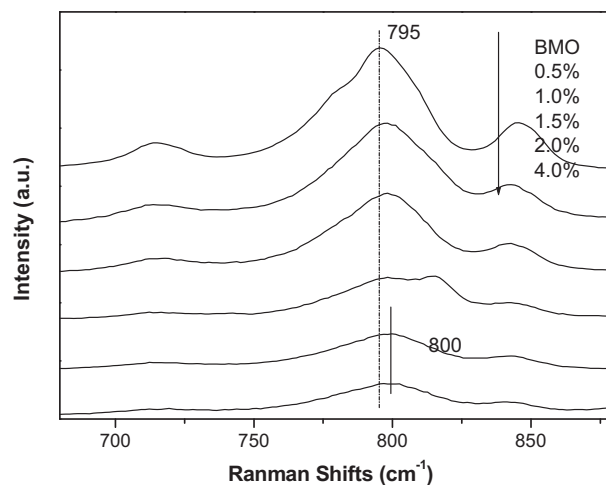


Fig. 5. Raman spectra of BMO and G-BMO composites.

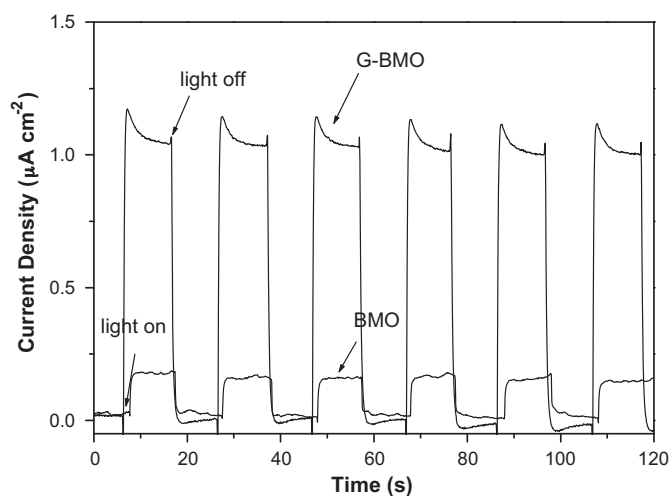


Fig. 6. Photocurrent transient responses of BMO and G-BMO electrodes. $[\text{Na}_2\text{SO}_4] = 0.1\text{ M}$.

ites. The observation of the gradual decrease in the bond lengths of the apical Mo-O distance strongly suggested the chemical interaction between Bi_2MoO_6 and graphene.

3.4. Mechanism of enhancement of visible photoactivity

Photoelectrochemical experiments were then performed to investigate the electronic interaction between Bi_2MoO_6 and graphene. Photocurrent measurements were carried out for Graphene- Bi_2MoO_6 (1.0 wt%) and Bi_2MoO_6 after deposition on ITO electrodes (Fig. 6). A fast and uniform photocurrent response was observed for each switch-on and switch-off event in both electrodes (Graphene- Bi_2MoO_6 and Bi_2MoO_6). The photocurrent transients had the different shape for each electrode. This photoresponsive phenomenon was entirely reversible. In the Graphene-BMO electrode, the electron-transfer characterization of graphene increased the charge separation process of the Helmholtz layer and changed the charge distribution of depletion layer available. Using the equivalent circuit, there was the constant phase elements (CPE) of the inner layer of the Graphene-BMO sample different from Bi_2MoO_6 electrode. And the photocurrent of Graphene-BMO electrode decreased slowly by reason of charging to the constant phase elements (CPE) of the inner layer of the Graphene-BMO sample. It was worthy to note that the pho-

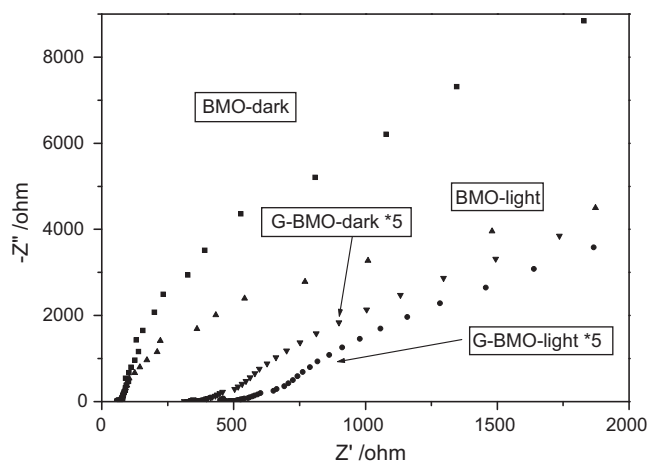


Fig. 7. Electrochemical impedance spectroscopy (EIS) Nyquist plots of BMO and G-BMO electrodes before and after visible light irradiation ($\lambda > 420$ nm). For better comparison the EIS Nyquist plot of G-BMO is shown with five times magnification.

photocurrent of the Graphene-Bi₂MoO₆ electrode was about six times as high as that of the Bi₂MoO₆ electrode which indicated that the separation efficiency of photoinduced electrons and holes was improved through the electronic interaction between graphene and Bi₂MoO₆. The ability of electron transfer from photocatalysts to the graphene sheet had been detected by time-resolved fluorescence spectroscopy in the Graphene-CdS nanocomposite [27].

To investigate the influence of graphene hybridization on the photoelectric property, the electrochemical impedance spectroscopy technology (EIS) was used to study the solid/electrolyte interfaces of Bi₂MoO₆ and Graphene-Bi₂MoO₆ samples. Fig. 7 showed the EIS Nyquist plots of Bi₂MoO₆ and Graphene-Bi₂MoO₆ electrodes before and after visible light irradiation ($\lambda > 420$ nm). The diameter of the arc radius on the EIS Nyquist plot of the Graphene-Bi₂MoO₆ electrode was smaller than that of the Bi₂MoO₆ electrode with or without visible light irradiation. The smaller the arc radius of the EIS Nyquist plot, the lower the electric charge transfer resistance. Using the equivalent circuit, the formation of photoinduced electron-hole pair in the Bi₂MoO₆ electrode reduced significantly the resistance of depleting layer (R_3) under visible light irradiation. And different from dark field, the Helmholtz layer was mainly occupied by the photoinduced electron-hole pair, so the electric charge transfer resistance (R_2) was also reduced. In the Graphene-BMO electrode, graphene on the surface increased the process of charge separation, influenced the distribution of the electrical double layer, and promoted the electron transfer, so that the electric charge transfer resistance (R_2) decreased significantly. The charge distribution of electrical double layer also impacted the depleting layer, so that R_3 decreased. In contrast with dark field, the electric charge transfer resistance (R_2) and the depleting layer resistance (R_3) also reduced under visible light irradiation. Because R_2 and R_3 in the Graphene-BMO electrode were much smaller than that in Bi₂MoO₆ electrode, the diameters of the arc radius on the EIS Nyquist plots of Bi₂MoO₆ electrodes decreased more evidently than that of the Graphene-BMO electrode. Thus, in the case of Graphene-Bi₂MoO₆, the photo-induced electron-hole pairs were easier separated and transferred to the sample surface which was due to the hybridization with graphene, i.e., the photoinduced electrons and holes were separated more efficiently through an interfacial interaction between graphene and Bi₂MoO₆.

It was important to identify the main oxidant in the photocatalytic degradation process to investigate the photocatalytic mechanism. Detecting the main oxidant could be carried out through the radicals and holes trapping experiments [28]. Fig. 8 showed the photodegradation of MB with the addition of holes and

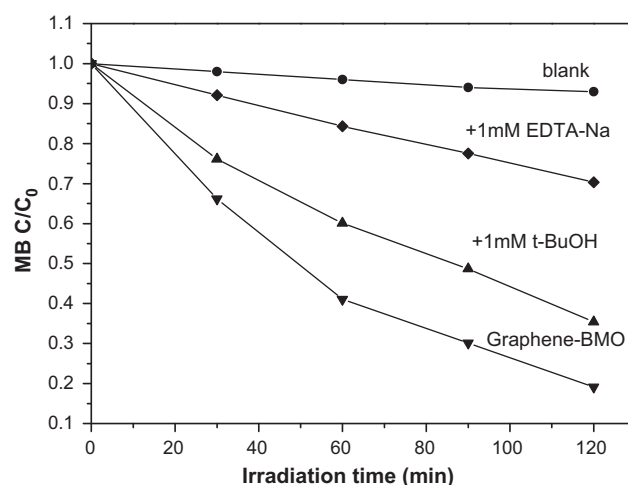


Fig. 8. Photocatalytic degradation of MB with the addition of hole and radical scavenger under visible light irradiation ($\lambda > 420$ nm).

hydroxyl radicals scavengers, respectively. The addition of 1 mM tert-butanol as hydroxyl radicals scavenger caused a minor change in the photocatalytic degradation of MB, while the MB could be greatly prevented by the addition of capture for holes (EDTA-Na). It clearly indicated that the free hydroxyl radicals were not the main active oxidative species of the Graphene-Bi₂MoO₆ photocatalysts, but the photocatalytic process was mainly governed by direct holes and O₂^{•-} oxidation reaction.

On the basis of the above results, the electronic interaction between graphene and γ -Bi₂MoO₆ was confirmed and the enhanced photocatalytic activity could be explained by the following mechanism: Photo-generated electrons and holes within the Bi₂MoO₆ either took part in redox reactions at the surface or recombined. The recombination process had a faster kinetics than the redox reactions and therefore controlled the efficiency of the photocatalytic process [29]. In the presence of graphene, photo-generated electrons were scavenged by graphene. Thus, the possibility of the recombination of electron-hole pairs decreases, leaving more hole charge carriers and promote the degradation of MB. Meanwhile, O₂ absorbed on the surface of graphene could accept e⁻ and form O₂^{•-} which then oxidized MB directly on the surface.

4. Conclusions

It has been demonstrated that graphene-hybridized γ -Bi₂MoO₆ nanoplates possessed significant visible light photocatalytic activity. The activity was increased by almost four times when loaded with 1.0 wt% graphene. The electronic interaction between graphene and γ -Bi₂MoO₆ was supposed to be responsible for the enhanced photocatalytic activity and photocurrent conversion. The graphene hybridization was proven to be a promising approach to develop highly efficient and stable photocatalysts under the visible light irradiation.

Acknowledgments

This work is supported by the National Natural Science Foundation of China (20925725), the National Basic Research Program of China (2007CB613303) and the Fundamental Research Funds for the Central Universities (2009QN047).

Appendix A. Supplementary data

Supplementary data associated with this article can be found, in the online version, at [doi:10.1016/j.molcata.2011.03.012](https://doi.org/10.1016/j.molcata.2011.03.012).

References

- [1] G.M. Liu, X.Z. Li, J.C. Zhao, H. Hidaka, N. Serpone, *Environ. Sci. Technol.* 34 (2000) 3982–3990.
- [2] R. Asahi, T. Morikawa, T. Ohwaki, K. Aoki, Y. Taga, *Science* 293 (2001) 269–271.
- [3] D. Chatterjee, S. Dasgupta, *J. Photochem. Photobiol. C: Photochem. Rev.* 6 (2005) 186–192.
- [4] Y. Shimodaira, H. Kato, H. Kobayashi, A. Kudo, *J. Phys. Chem. B* 110 (2006) 17790–17797.
- [5] J. Ricote, L. Pardo, A. Castro, P. Millan, *J. Solid State Chem.* 160 (2001) 54–61.
- [6] Y. Man, R.L. Zong, Y.F. Zhu, *Acta Phys. Chim. Sin.* 23 (2007) 1671–1676.
- [7] X. Zhao, T.G. Xu, W.Q. Yao, Y.F. Zhu, *Appl. Surf. Sci.* 255 (2009) 8036–8040.
- [8] L.W. Zhang, T.G. Xu, X. Zhao, Y.F. Zhu, *Appl. Catal. B: Environ.* 98 (2010) 138–146.
- [9] K. Woan, G. Pyrgiotakis, W. Sigmund, *Adv. Mater.* 21 (2009) 2233–2239.
- [10] Y.Y. Li, J.P. Liu, X.T. Huang, J.G. Yu, *Dalton Trans.* 39 (2010) 3420–3425.
- [11] H.B. Fu, T.G. Xu, S.B. Zhu, Y.F. Zhu, *Environ. Sci. Technol.* 42 (2008) 8064–8069.
- [12] S.B. Zhu, T.G. Xu, H.B. Fu, J.C. Zhao, Y.F. Zhu, *Environ. Sci. Technol.* 41 (2007) 6234–6239.
- [13] L.W. Zhang, H.B. Fu, Y.F. Zhu, *Adv. Funct. Mater.* 18 (2008) 2180–2189.
- [14] L.W. Zhang, H.Y. Cheng, R.L. Zong, Y.F. Zhu, *J. Phys. Chem. C* 113 (2009) 2368–2374.
- [15] M. Ishigami, J.H. Chen, W.G. Cullen, M.S. Fuhrer, E.D. Williams, *Nano Lett.* 7 (2007) 1643–1648.
- [16] C. Berger, Z. Song, X. Li, X. Wu, N. Brown, C. Naud, D. Mayou, T. Li, J. Hass, A.N. Marchenkov, E.H. Conrad, P.N. First, W.A. deHeer, *Science* 312 (2006) 1191–1196.
- [17] E. Bekyarova, M.E. Itkis, P. Ramesh, C. Berger, M. Sprinkle, W.A. deHeer, R.C. Haddon, *J. Am. Chem. Soc.* 131 (2009) 1336–1337.
- [18] G. Williams, B. Seger, P.V. Kamat, *ACS Nano* 2 (2008) 1487–1491.
- [19] H. Zhang, X.J. Lv, Y.M. Li, Y. Wang, J.H. Li, *ACS Nano* 4 (2010) 380–386.
- [20] G. Williams, P.V. Kamat, *Langmuir* 25 (2009) 13869–13873.
- [21] W.S. Hummers, R.E. Offeman, *J. Am. Chem. Soc.* 80 (1958), 1339–1339.
- [22] D. Wang, D. Choi, J. Li, Z. Yang, Z. Nie, R. Kou, D. Hu, C. Wang, L.V. Saraf, J. Zhang, I.A. Aksay, J. Liu, *ACS Nano* 3 (2009) 907–914.
- [23] D. Li, M.B. Muller, S. Gilje, R.B. Kaner, G.G. Wallace, *Nat. Nanotechnol.* 3 (2008) 101–105.
- [24] H.H. Li, C.Y. Liu, K.W. Li, H. Wang, *J. Mater. Sci.* 43 (2008) 7026–7034.
- [25] R. Murugan, *Phys. B* 352 (2004) 227–232.
- [26] D.H. Franklin, E.W. Israel, *J. Phys. Chem.* 95 (1991) 10763–10772.
- [27] A. Cao, Z. Liu, S. Chu, M. Wu, Z. Ye, Z. Cai, Y. Chang, S. Wang, Q. Gong, Y. Liu, *Adv. Mater.* 22 (2010) 103–106.
- [28] T.L. Xu, Y. Cai, K.E. O'Shea, *Environ. Sci. Technol.* 41 (2007) 5471–5477.
- [29] M.R. Hoffmann, S.T. Martin, W.Y. Choi, D.W. Bahnemann, *Chem. Rev.* 95 (1995) 69–96.